Africa Journal of Geosciences

Refereed scientific journal

Volume 1, 2018

ISSN: 1858-8913 (online), 1858-8905 (hard copy), http://www.iua.edu.sd

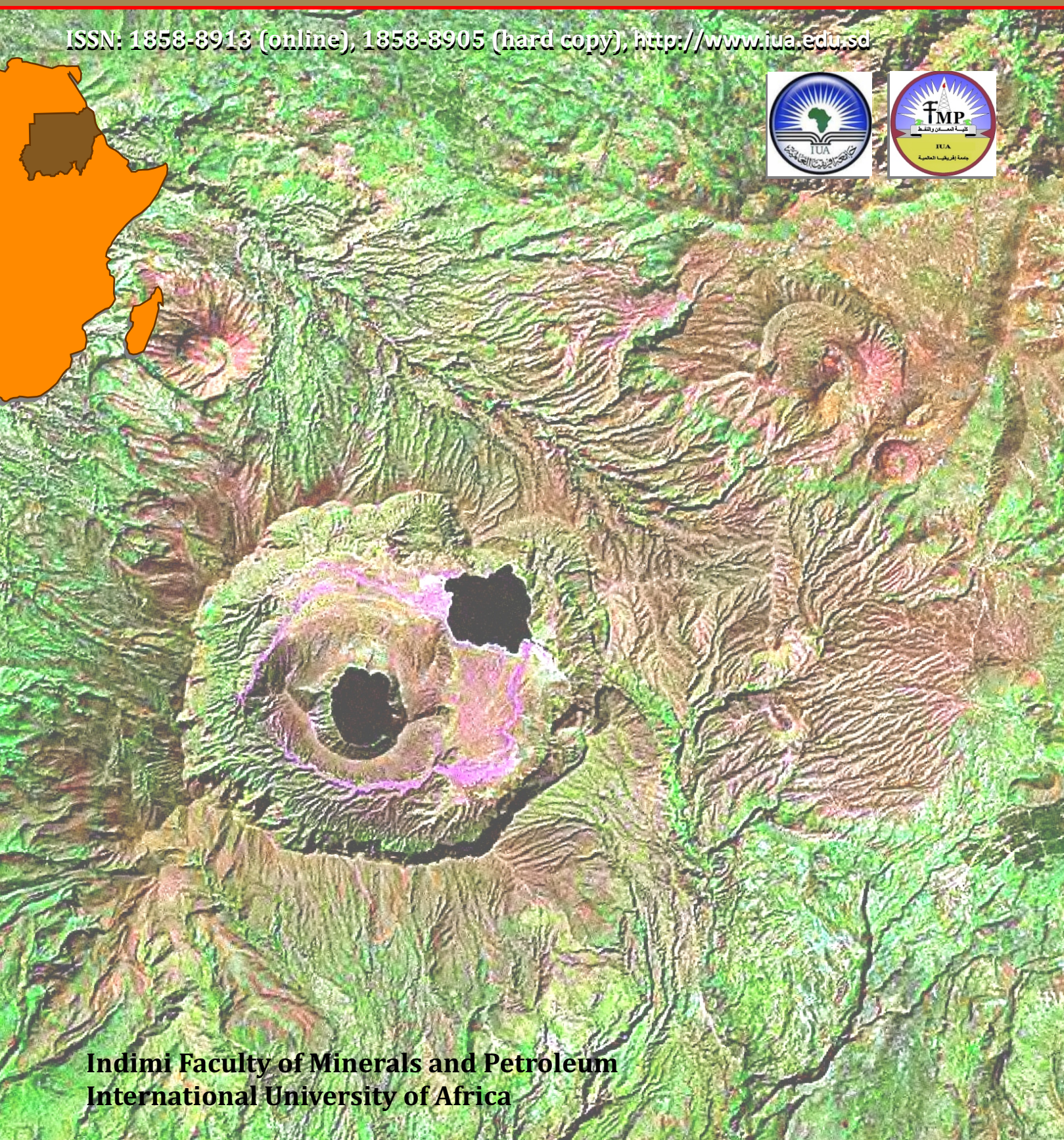

Indimi Faculty of Minerals and Petroleum
International University of Africa

مجلة افريقيا لعلوم الأرض

مجلة علمية محكمة

المجلد الأول ، ٢٠١٨

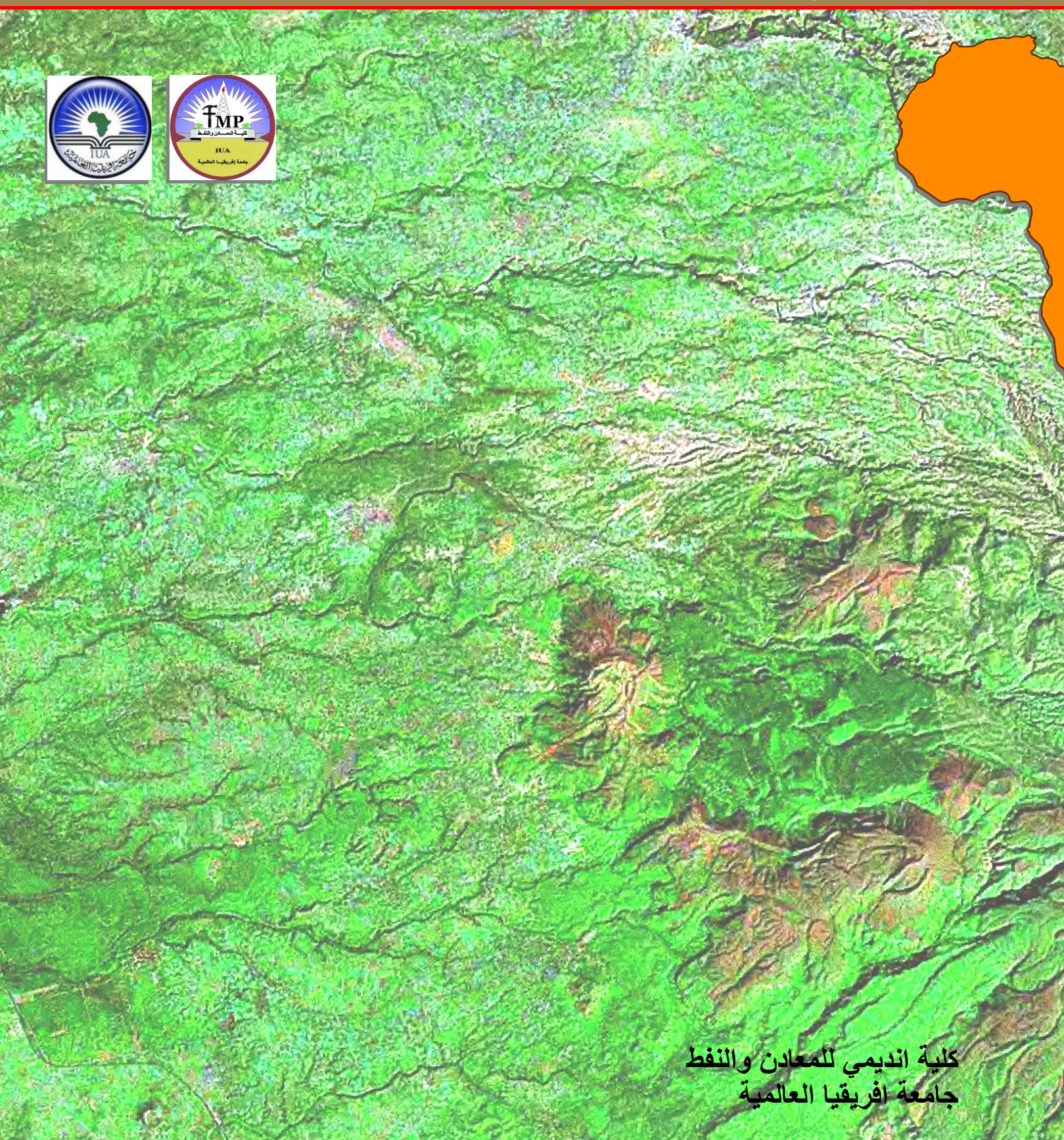

كلية انديمي للمعادن والنفط
جامعة افريقيا العالمية

Africa Journal of Geosciences (AJG)
Vol. 1, 2018
ISSN: 1858-8913 (online), 1858-8905 (hard copy), http://www.iua.edu.sd

Spectral Analysis of ASTER Data for Hydrothermal Alteration Mapping in Lesbab Area, the Northern State, Sudan

Fadlallah, H.H.A. and Elsayed Zeinelabdein, K.A.

Department of Geology, Al Neelain University, Khartoum, Sudan
E-mail: khalid.elsayed@gmail.com

Received: 06 November 2018/ revised: 06 December 2018 / accepted: 20 December 2018

Abstract

Hydrothermal alteration zones, which are related to mineralization, can be identified and discriminated based on distinctive spectral properties that appears in ASTER satellite data**.** The aim of this study is to conduct mineral prospecting utilizing the semi-hyperspectral ASTER data to enhance and delineate the hydrothermal alteration zones in Lesbab area of the Northern State. The effectiveness of the spectral analysis techniques used in this study lies in their ability to compare a pixel spectrum with the spectra of known pure materials. A variety of techniques are available for selecting and extracting the pixels that portray pure materials from the ASTER dataset. The adopted spectral endmember extraction procedures include the Minimum Noise Faction (MNF), Pixel Purity Index (PPI) and n-dimensional visualization. The extracted endmembers were compared and correlated with the spectral library spectra. The mapping was carried out utilizing the Spectral Angle Mapper (SAM), Linear Spectral Unmixing (LSU), and Mixture Tuned Matched Filtering (MTMF) classification techniques. Accordingly, **t**he mineral indices of hematite, Alunite, Kaolinite and Muscovite mapped. The outcome of the study revealed that the LSU technique well-discriminate the desired minerals and provide better mapping of the alteration zones among the utilized techniques. Chemical analysis disclosed the presence of gold within the alterations zones, with Au concentration ranges from 1.1 to 15 ppm. Thus, the chemical analysis provide support to the results obtained through the means of remote sensing and GIS investigations. These results encourage the use of remote sensing and GIS techniques in future studies for mineral deposits.

Keywords: Alteration, Spectral Analysis, ASTER, PPI, SAM, LSU, MTMF, Lesbab Area.

1. Introduction

The national endeavors devoted to raising the living standard the industrialization of the country laid a swelling pressure on mineral resources. The increasing demand for mineral resources and the scarcity of these minerals speed up the search for new and effective techniques that help in discovering new mineral reserves.

Exploitation of remote sensing in mineral exploration is well understood via geological mapping and delineation of the regional and local spectral and structural features. Ore deposits are identified through the detection of the hydrothermally altered rocks by their spectral signatures (Qiu et al., 2006; Gupta, 2003; Sabins, 1999).

The present work demonstrates the capabilities of optical multispectral ASTER Visible and Near Infrared (VNIR) and Shortwave Infrared (SWIR) data in terms of mineral indices and spectral analysis to demarcate the alteration zones related to mineralization as large scale exploration investigations in the study area.

The study area is located in the Northern State of Sudan. It is bounded by latitudes: 20^0 45′00″ - 21^0 00′00″ and longitudes: 32^0 00′00″ - 32^0 09′00″ (Fig. 1).

2. Tectonic and Geological Settings

The study area lies in the Wadi Halfa terrane of the Arabian Nubian Shield, comprising reworked eastern foreland of the Archean? Nile craton (meta-craton) and Proterozoic juvenile rocks of the Arabian Nubian Shield. The Wadi Halfa area is poorly understood due to the limited studies conducted in the area (Stern, 1994).

The Precambrian geology in NE Africa comprises two distinct crustal domains: The Nile craton and the Arabian-Nubian Shield. The Nile craton is dominated by heterogeneous gneisses and supra-crustal metasediments of pre-Neoproterozoic ages and ensialic geochemical affinities. The Nile craton has been pervasively remobilized during the Neoproterozoic Pan African. The western and the southern extensions of the Nile craton are not precisely defined.

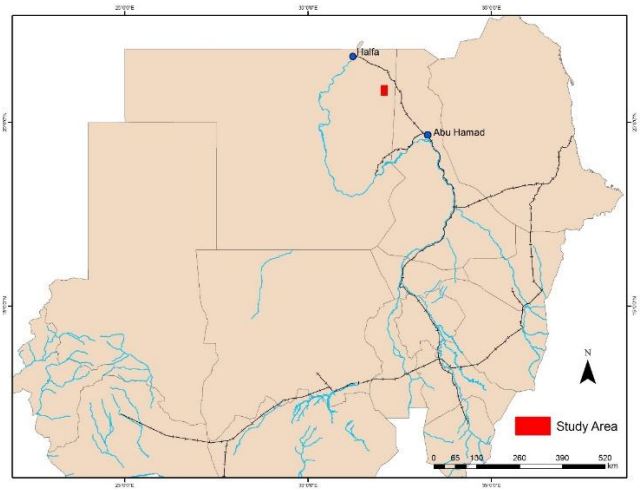

Fig. 1. Location map of the study area.

The whole region of N and NE Sudan seems likely to have been under mechanical and thermal instability during Pan-African orogeny, documented by presence of series of intense folding, faulting, shearing and magmatism with resultant wide spread and multi directional movements (Abdelsalam and Stern, 1993). The Nubian Shield in the north of Sudan is represented by the Gabgaba Terrane and the Nile craton is represented by the Bayuda and Wadi Halfa Terranes (Schandelmeier et al., 1994).

According to the previous studies in N and NE Sudan, the lithostratigraphic units of Wadi-Halfa-Bayuda-Gabgaba area are reported in the following sequence: high-grade gneiss (oldest), high-grade supra-crustal metasediments, low-grade metasediments, ophiolitic melange rocks, volcano-sedimentary sequences, molasse-type sediments, magmatic rocks and phanerozoic sediments (Denker et al., 1994; Abdelrahman, 1993; Vail, 1988; Barth and Meinhold, 1979).

3. Methodology

Advanced Space-borne Thermal Emission and Reflectance Radiometer (ASTER) is a cooperative effort between NASA and Japan. It records solar radiation in 14 spectral bands. This instrument provides enhanced capabilities for mineral exploration, measures reflected radiation in three bands between 0.52-0.86 µm (VNIR) and in six bands from1.6 to 2.43 µm (SWIR), with 15 and 30 m resolution, respectively. In addition, emitted radiations are measured at 90-m resolution in five bands in the range 8.125–11.65 µm wavelength regions (TIR; Yamaguchi et al., 1998; ASTER, 2001). The ASTER data used in this study are level 1T (AST_L1T). The data is acquired on Jan 11, 2005.

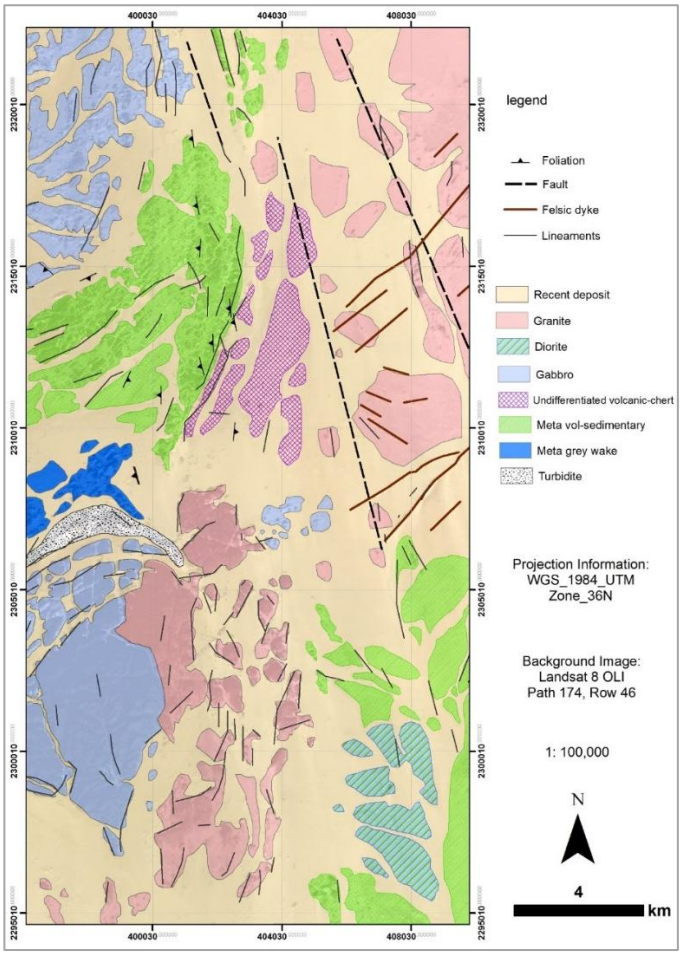

Fig. 1. Geological map of the study area.

The VNIR and SWIR data were then resampled, so that all 9 bands have the same 15×15 m pixel size, and subset the area corresponding to the specified study area.

The Internal Average Relative Reflectance (IARR) method has been applied to the VNIR and SWIR ASTER bands to correct it from the atmospheric or equipment related errors recorded on the image and analyze radiance data to obtain reflectance image.

The standard United States Geological Survey (USGS) spectral library has been convolved with the spectral response function and resembled, according to the band widths and distribution of the ASTER VNIR and SWIR nine bands.

Endmember extract was conducted using minimum noise fraction (MNF), pixel purity index (PPI) and n-dimensional visualization. Utilizing the spectral analyst, the extracted endmembers were identified and matched with the spectral library mineral spectra. These endmembers were correlated with remote sensing data, while the individual alteration minerals were mapped using the Spectral Angle Mapper (SAM), Linear Spectral Unmixing (LSU), and Mixture Tuned Matched Filtering (MTMF) classification algorithms. The adopted methodology is diagrammatically illustrated in Figure (2).

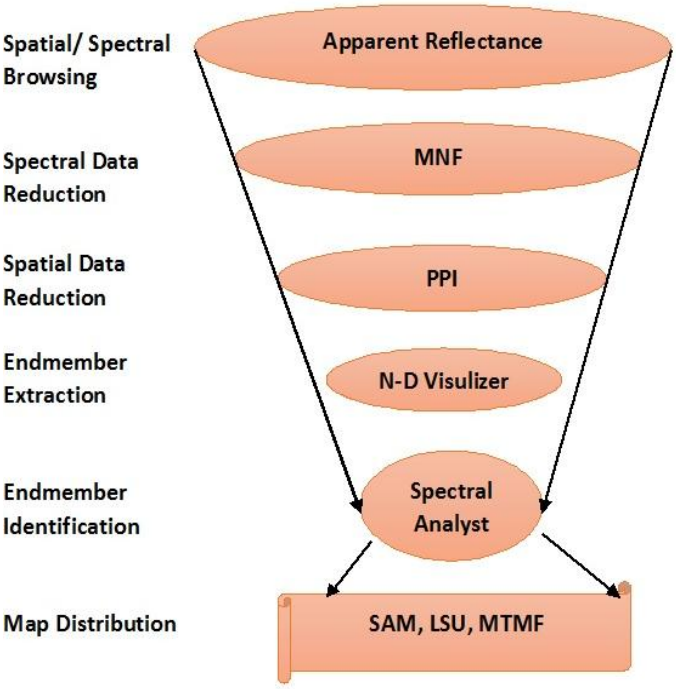

Fig. 2. Spectral Processing flow chart.

4. Result and Discussion

Many commonly used spectral image analysis techniques are based on the fact that remotely sensed imagery is sampled with numerous spectral bands at narrow bandwidths, making it possible to construct a spectrum for each pixel in the image. The spectrum can then be compared with the spectra of known pure materials such as minerals.

To effectively extract endmembers from high dimensional remote sensing data and to effectively process the data, it is often necessary that the dimensionality of the original data be decreased and noise in the data be segregated first. So the visualizing complexity and computational requirement for the subsequent analyses can be reduced. This is often achieved by applying a minimum noise fraction (MNF) transform to the high dimensional data. Once the inherent dimensionality of the image data is determined using the MNF transform, endmembers can then be derived by using PPI and n-dimensional visualization techniques from the higher-order MNF eigen images. These endmembers can be compared subsequently with the remote sensing data to determine the surface materials of each pixel by employing each of the spectral analysis algorithms, such as spectral angle mapper (SAM), and linear spectral unmixing (LSU), and Mixture Tuned Matched Filtering (MTMF).

4.1 Spectral resampling

The USGS mineral spectra is acquired in laboratory using spectrometers that are characterized by very high spectral resolution in the range of 10 nanometers. These spectra are measured from the wavelength of 0.4 to 2.5 µm (400 – 1500 nm). The selected mineral spectra are presented in Figure (3).

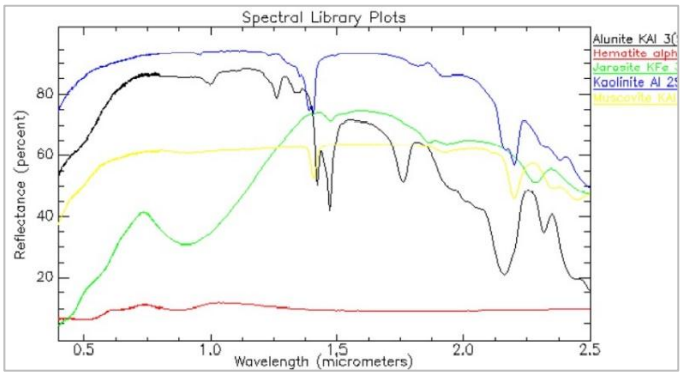

Fig. 3. Spectral library with ASTER of the USGS Spectra for the alteration minerals.

The range (0.4-2.5 µm) is covered by nine spectral bands of ASTER semi-hyperspectral sensor. Accordingly, in order to execute reasonable comparison between the USGS mineral spectral the pixel spectra extracted from ASTER data, a convolution process has been performed to resample the USGS spectra to the wavelength of ASTER. The resamples version of the spectra is presented in Figure (4).

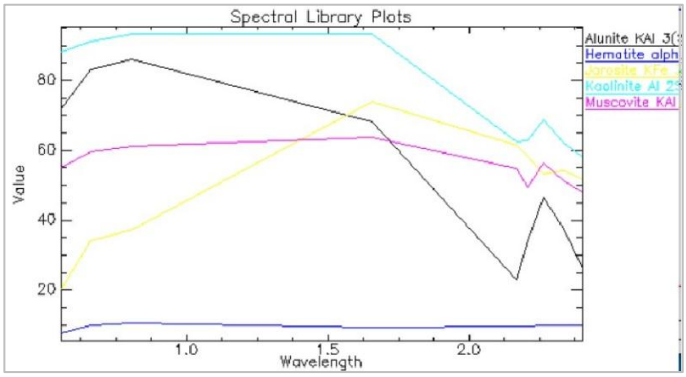

Fig. 4. Spectral resampling with ASTER and USGS Spectral library for the alteration minerals.

4.2 Endmember extraction

Spectra of the image could be extracted utilizing the "spectral end-member selection" procedures such as minimum noise fraction (MNF), pixel purity index (PPI) and n-dimensional visualization.

4.2.1. Minimum Noise Fraction (MNF)

The MNF transform was applied to the ASTER data to achieved a reasonable separation of coherent signal from complementary noise. Therefore, the MNF transformed eigen images were employed and coupled with pixel purity index and n-dimensional visualization techniques to facilitate the extraction of the endmembers. As in many other techniques, decorrelation and scaling of the noise in the MNF transform provide good insight into the relationship between different endmembers of the image and their spatial distribution of coherency.

In a common practice, MNF components with eigenvalues less than 1 are usually excluded from the data as noise in order to improve the subsequent spectral processing results, since eigen images with near-unity eigenvalues are normally noise-dominated (Jensen, 2005).

MNF transformation has been executed with the frame of the present study as preparatory step for selecting pixel with pure land cover types, that hopefully be correlated with one of the resampled USGS mineral spectra. This process is intended to reduce the noise inherent in the image to aid in selecting the pure pixels. The eigenvalues of the transformed ASTER 9 bands are presented in Figure (5).

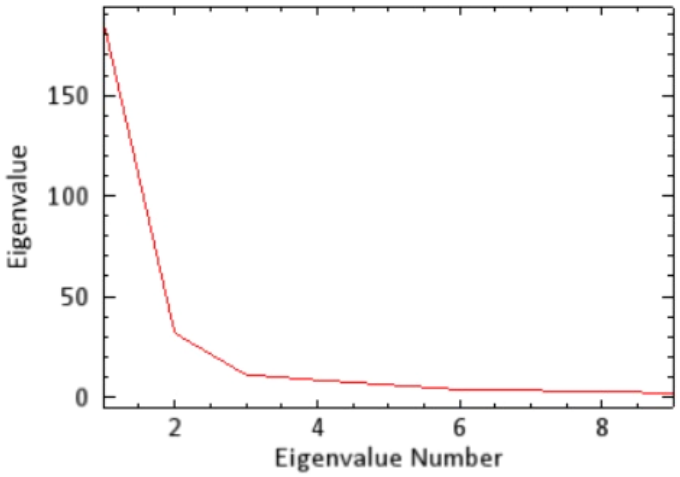

Fig. 5. The MNF eigenvalues plot of the 9 eigenvalues of the ASTER data.

4.2.2. Pixel purity index (PPI)

Identifying endmember pixels whose spectra are extreme (or spectrally pure) is not a simple task, especially in high-dimension image datasets. This is because most pixels often contain varying proportions of different materials of more than one type. Unlike training sites in multispectral data, which are usually arithmetic mean spectral vectors that can be selected easily manually or with regional growth tools (Jensen, 2005).

Pixel purity index (PPI) is a means to determine automatically the relative purity of the pixels from the higher order MNF eigenvalues using the convex geometry argument (Boardman, 1993; Boardman et al., 1995). By repeatedly projecting n-dimensional scatter plots of the MNF images onto a random unit vector, a PPI image is formed in which the digital number (DN) of each pixel corresponds to the total number of times that the pixel was judged as ‘‘extreme’’ (i.e., falling onto the ends of the unit vector) in all projections. Typically, the brighter pixel in the PPI image, the higher relative purity because it was more frequently recorded as being a spectrally extreme pixel. To reduce the number of pixels to be analyzed for endmember determination and to facilitate the separation of purer materials from mixed, a 10,000-projection of the scatter plot and a threshold factor of 2.5 is applied to the PPI image to select the purest PPI pixels. The results of this process is displayed in Figure (6).

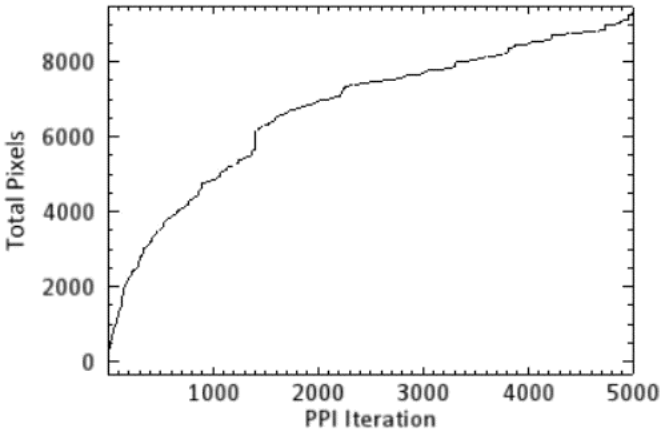

Fig. 6. The PPI plot showing 10,000 of PPI pixels and 5,000 of PPI iterations.

4.2.3. n-Dimensional endmember visualization

After applying PPI thresholding, the data volume to be analyzed has been effectively reduced. However, it is still possible that many less ‘‘pure’’ pixels have crept in as candidate endmembers during the automatic selection process. To further refine the selection of the most spectrally pure endmembers from the derived two-dimensional PPI image and more importantly, to label them with specific endmember types (i.e., to assign these endmembers to specific alteration types), it is essential to reexamine visually the selected pixels in the n-dimensional feature space and to assign them manually to appropriate types (Boardman, 1993).

This is accomplished by using two or more MNF eigen images to form the n-dimensional scatter plot. All the pixels that were previously selected using the PPI thresholding procedure are displayed as pixel clouds in the n-dimensional spectral space. To make possible the visualization of a scatter plot with more than two dimensions, the pixel clouds of high dimensions are cast on the two-dimensional display screen. With interactive rotation and visualization by an image analyst in the spectral space, the convex corners of the pixel clouds can be located and designated as the purest spectral endmembers. As a result, the number of endmembers to be analyzed is further reduced.

The actual spatial locations of these final spectral endmembers are then determined in the two-dimensional image space of the MNF or the original dataset, and they are labeled with the specific endmember types for these locations. The pixel values of all the 9 MNF eigen images are used to form a display of the n-dimensional visualization projection of the PPI thresholded pixels. For the ASTER dataset covering the study area, five major types of endmembers were extracted.

4.3 Identification of Endmembers and Mapping

Identifying materials can often be a very difficult process. It is further complicated by the fact that an image-derived endmember may be a mixture of more than one material. In this study, the spectral analysis has been used to identify the endmembers extracted, and also common sense was used with results and compare the output of the spectral analysis with the spectral library spectra to measure the similarities.

The spectral Analysis is intended to compare the input spectra, such as the endmember spectra to a spectral library of known materials (Adams et al., 1995). Several different comparison methods are available for use. The spectral analysis returns a score for each spectrum in the library. The highest scores are returned for the library spectra that best match the input spectrum. If the Spectral Library does not contain a spectrum for the material corresponding to the input spectrum, then the spectral analysis returns low scores. The obtained scores for the analyzed spectra are presented in Table (1).

Table 1. The score of materials by spectral analyst:

Type	Score
Hematite	0.75
Alunite	0.81
Muscovite	0.97
Kaolinite	0.74

The endmembers can be compared subsequently with the remote sensing data to determine the surface materials of each pixel by employing one of the spectral analysis algorithms, such as spectral angle mapper (SAM), linear spectral unmixing (LSU) and Mixture Tuned Matched Filtering (MTMF). The methodology of the spectral image analysis techniques applied to the ASTER data are explained below, and the results from these techniques are described and compared with each other.

4.3.1. Spectral Angle Mapper (SAM)

SAM is a whole - pixel classification method used for comparing image spectra (an unknown) to known reference spectra. The SAM techniques estimate the similarity between the image spectrum and the reference spectrum by calculating the angle between the two spectra while treating them as vectors in n-dimensional space. Four endmembers were selected from the spectral library. These included alunite, kaolinite, muscovite, and hematite. Maximum radian angle of 0.10 was set. The result of the SAM classification process is shown in Figure (7), which depicts alunite as yellow pixels, kaolinite as blue, muscovite as green, and most of the pixels are classified as hematite displayed in red colour.

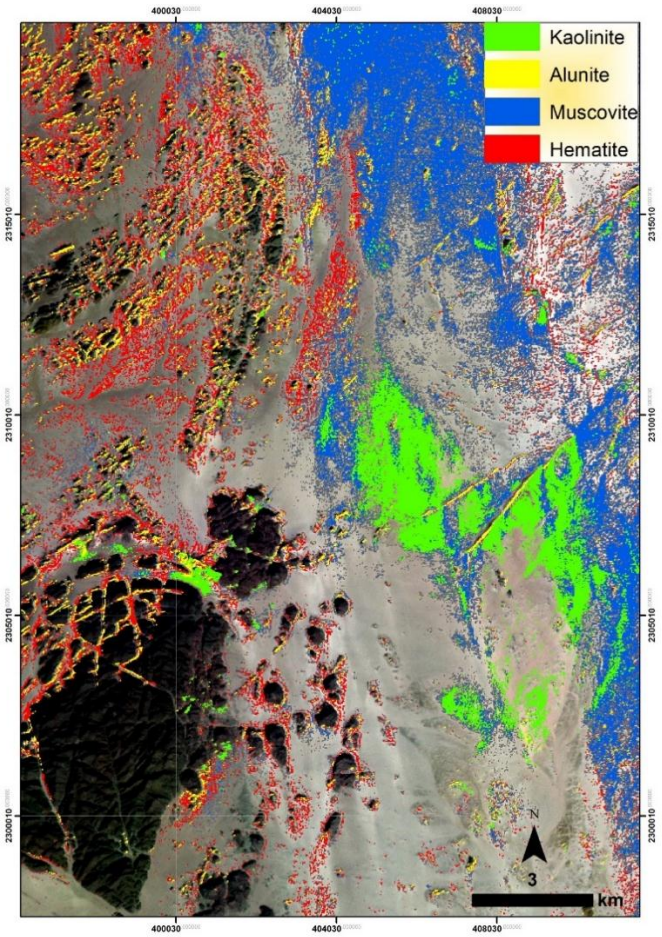

Fig. 7. Alteration minerals maps obtained through SAM classification**.**

4.3.2. Linear Spectral Unmixing (LSU)

Linear spectral unmixing is a sub-pixel method which determines relative abundances of materials that are depicted in multi- or hyperspectral imagery based on the materials spectral characteristics. The reflectance at each pixel of the image is assumed to be a linear combination of the reflectance of each endmember present within the pixel. Sub-pixel analysis methods can be used to calculate the quantity of target materials in each pixel of an image. The results of spectral unmixing appear as a series of gray-scale images, one for each endmember, plus a root-mean-square (RMS) error image. Higher abundances (and higher errors for the RMS error image) are represented by brighter pixels. The unmixing results should have a data range (representing endmember abundance) from 0-1. However, negative values and values greater than one are possible (Van Der Meer, 1995).

The result of the LSU is shown in Figure (8) that depicts alunite, kaolinite, muscovite and hematite as yellow, blue, green and red colors, respectively. However, the numbers of pixels known are lower in LSU as compared with SAM classification results. This method is also useful for determining the abundance of each matter in the pixel. The result of this method is considered as the best results obtained during this study.

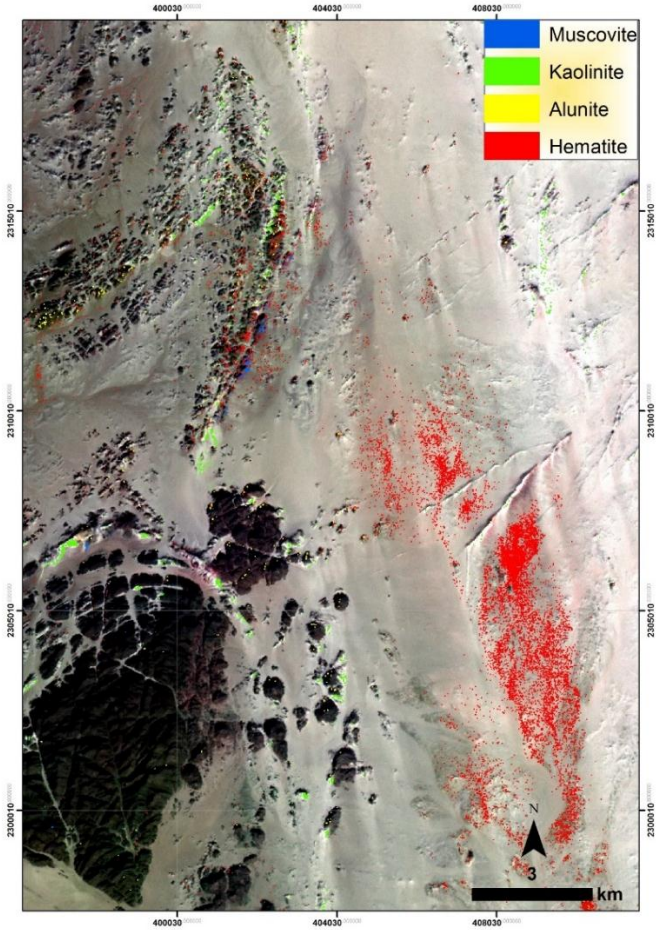

Fig. 8. Final classification image maps for Linear spectral unmixing.

4.3.3. Mixture Tuned Matched Filtering (MTMF)

MTMF is a combination of linear spectral unmixing and matched filter (MF) models that map the target abundances in the presence of an unknown spectrum of mixed background. In this method, it is not necessary that spectral characteristics of the background materials are known. The calculation of minimum noise fraction (MNF) for input data is necessary for the MTMF algorithm. In this method, the pure pixels with spectra similar to that of the target spectra are identified in the first step. Then, the pure pixels that have no close matching with the target spectra are identified as infeasibility values and are used for the determination of the background spectrum. Finally, the values of target fractions and background spectra are determined. The results of this algorithm are available as MF and infeasibility. By comparison of data from these two images in a two-dimensional space, it is possible to select the pixels with high MF and low infeasibility and also to evaluate the mapping process (Boardman et al., 1995; Boardman, 1998).

The result of the MTMF is presented in Figure (9) that depicts alunite, kaolinite, muscovite and hematite as yellow, blue, green and red colors, respectively.

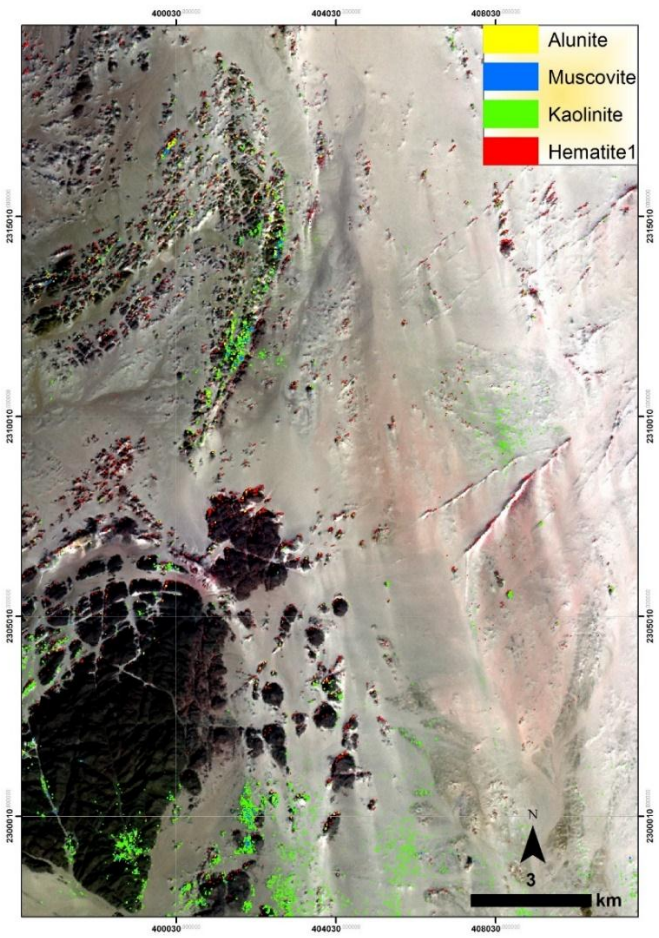

Fig. 9. Final classification image maps for Mixture Tuned Matched Filtering MTMF.

Despite the slight differences in the results of the above tried techniques, the overall outcome revealed that the study area is rich in alteration minerals. This may be produced by the intrusion of hydrothermal solutions that render the area quite prospective for mineral deposits. Accordingly, a number of chip samples were collected during the field work from or close to the alteration zones. The chemical analysis of these samples disclosed the presence of gold within these samples. the Au concentration ranges from 1.1 to 15 ppm. Thus, the chemical analysis provide support to the results obtained through the means of remote sensing and GIS investigations.

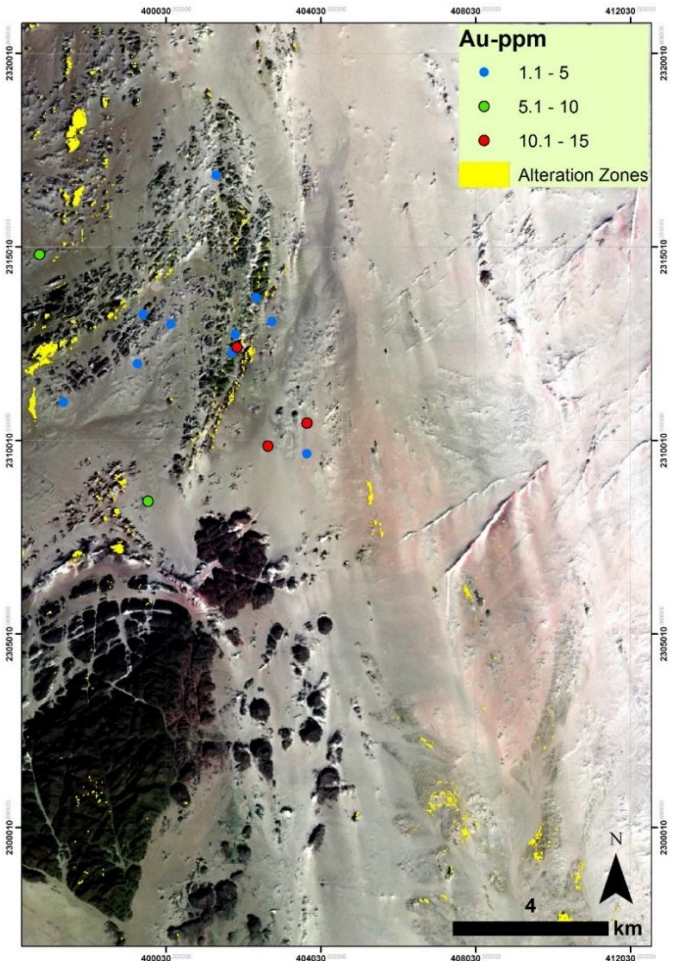

Fig.10. Alteration Map with geochemical chip samples**.**

5. Conclusions

The spectral analysis techniques were implemented based on the comparison of a pixel spectrum with the spectra of known pure materials, which were effectively extracted using endmember selection procedures such as minimum noise fraction or (MNF), pixel purity index (PPI) and n-dimensional visualization.

Three spectral analysis procedures, including spectral angle mapper (SAM), spectral feature fitting (SFF) and linear spectral unmixing (LSU) were applied to the ASTER data. The utilized techniques managed to discriminate the alteration minerals to variable degrees of success. Among the applied methods, LSU gave the best results, and provided an accurate discrimination of mineral indices such as alunite, kaolinite, muscovite and hematite. Similar results were obtained by Abubakr et al. (2017). Accordingly, the obtained results are considered reliable, since chemical analysis disclosed the presence of gold within the outlined alterations zones, with Au concentration ranges from 1.1 to 15 ppm. Thus, the chemical analysis provide support to the results obtained through the means of remote sensing and GIS investigations. These results encourage the use of remote sensing and GIS techniques in

future studies for mineral deposits, however, further researches are recommended in other geological environments.

References

Abdelrahman E. M. (1993). Geochemical and geotectonic controls of the metallogenic evolution of selected ophiolite complexes from the Sudan.

Abdelsalam, M.G., Stern, J. (1993). Timing of events along the Nakasib suture and the Oko shearz one, Sudan. In: THORWEIHUE., & SCHANDELMEIHER (eds.) Geoscientijic Research in Northeast Africa, Balkema, 99-103.

Abubakar, A.J., Hashim, M., Pour, A.B. (2017). Spectral mineral mapping for characterization of subtle geothermal prospects using ASTER data. Application to land cover change in the Brazilian Amazon. Remote Sensing of Environment 52, 137–154.

Adams, J.B., Sabot, D.E., Kapos, V., Almeida, F., Roberts, D.A., Smith, M.O., Gillespie, A.R., (1995). Classification of multispectral images based on fractions of endmembers:

ASTER (2001). User guide

Barth, H. and Meinhold, K. D. (1979). Sudanese German Exploration Project. Technical Report, Part I: Mineral prospecting in the Bayuda Desert. Vol. A: Investigation of Mineral Potential, Unpubl. Rep., BGR, Hannover.

Boardman J.W. (1998). Leveraging the high dimensionality of AVIRIS data for improved sub-pixel target unmixing and rejection of false positives: mixture tuned matched filtering. Summaries of the Seventh Annual JPL Airborne Geoscience Workshop, Pasadena.

Boardman, J.W., Kruse, F. A., and Green, R. O. (1995). Mapping target signatures via partial unmixing of AVIRIS data: in Summaries, Fifth JPL Airborne Earth Science Workshop, JPL Publication 95-1, v. 1, p. 23-26.

Boardman. J.W. (1993). Automating spectral unmixing of AVIRIS data using convex geometry concepts. In: Summaries of the 4th Annual JPL Air-borne Geoscience Workshop, Pasadena, pp. 11–14.

Denkler, T., Franz, G., Schandelmeier, H. (1994). Tectonometamorophic evolution of the Neoproterozoic Delgo-Atmur zone, northern Sudan. Geologische Rundschau, 83, pp. 578-590.

Griffiths et al., 1987

Gupta, R. (2003). Remote Sensing Geology. 2nd ed. Springer-Verlag, Berlin Heidelberg, Germany**.**

Jensen, J.R. (2005). Introductory Digital Image Processing. Person Prentice Hall, Upper Saddle River, p. 526.

NASA ASTER (2004). Advanced Spaceborne Thermal Emission and Reflection Radiometer. Available from: http://asterweb. jpl.nasa. gov.

Qiu, F., Abdelsalam, M.G., Thakkar, P. (2006). Spectral analysis of ASTER data covering part of the Neoproterozoic Allaqi-Heiani suture, Southern Egypt.

Sabins, F.F. (1999). Remote sensing for mineral exploration. Ore Geol. Rev. 14, 157 -183.

Schandelmeier, H., Wipfler, E., Küster, D., Sultan, M., Beckler, R., Stern, R. J., Abdel Salam, M.G. (1994). Atmur-Delgo suture: a Neo-Proterozoic oceanic basin extending into the interior of northeast Africa. Geology 22, 563-566

Stern, R.J. (1994). Arc assembly and continental collision in the Neoproterozoic East African Orogen: implications for the consideration of Gondwanaland. Annual Reviews Earth and Planetary Science Letters 22, 319–351.

Vail, J.R., 1988. Lexicon of geological terms for the Sudan. Amsterdam: A.A. Balkema. 199 pp.

Van der Meer F. (1995). Spectral mixture modelling and spectral stratigraphy in carbonate lithofacies mapping ISPRS journal of photogrammetry and remote sensing 51(3) 150.

Yamaguchi, Y., Kahle, A.B., Kawakami, T. and Paniel, M. (1998). Overview of the advanced space borne thermal emission and reflection radiometer (ASTER). IEEE Transaction on Geoscience and Remote Sensing, 36 (4), 1062–1071.